

Simulations of biological production in the Rhodes and Ionian basins of the eastern Mediterranean

Ernesto Napolitano ^a, Temel Oguz ^{b,*}, Paola Malanotte-Rizzoli ^c, Aysen Yilmaz ^b, Emilio Sansone ^a

^a *Institute of Meteorology and Oceanography, Istituto Universitario Navale, Naples, Italy*

^b *Middle East Technical University, Institute of Marine Sciences, Erdemli 33731, Icel, Turkey*

^c *Massachusetts Institute of Technology, Department of Earth, Atmospheric and Planetary Sciences, Cambridge, MA 02139, USA*

Received 3 March 1999; accepted 27 July 1999

Abstract

The biological production characteristics of the Rhodes and western Ionian basins of the eastern Mediterranean are studied by a one-dimensional, coupled physical–biological model. The biological model involves single aggregated compartments of phytoplankton, zooplankton, detritus as well as ammonium and nitrate forms of the inorganic nitrogen. It interacts with the physical model through the vertical eddy diffusivity which is calculated using the Mellor–Yamada level 2.5 turbulence parameterization. The model simulations demonstrate the importance of the contrasting physical oceanographic characteristics of these two basins on affecting their yearly planktonic structures. The annual primary production in the Rhodes basin is estimated as $\sim 97 \text{ g C m}^{-2} \text{ yr}^{-1}$ which is comparable with the northwestern Mediterranean. The western Ionian basin, on the contrary, possesses only 10% of the Rhodes' productivity and therefore represent a most oligotrophic site in the eastern Mediterranean. The Rhodes basin reveals a strong bloom in early spring, typically in March, a weaker bloom in early winter, typically in January, and a subsurface production below the seasonal thermocline during summer. This structure is slightly modified in the western Ionian basin, and the early winter and early spring blooms are merged to cover the entire winter. These results are supported favorably by the available observations both in their magnitudes and timing. © 2000 Elsevier Science B.V. All rights reserved.

Keywords: Eastern Mediterranean; Rhodes gyre; Western Ionian gyre; ecosystem modeling; primary production

1. Introduction

Contrary to the recent advances in the knowledge of the eastern Mediterranean physical characteristics, its biogeochemistry remains poorly documented and

unexplored except in some localized regions. Even the measurements of basic parameters such as chlorophyll *a* and nutrients are very sparse and mainly restricted to coastal areas, therefore far from providing clear temporal and spatial distributions. From the modeling perspective, the three-dimensional nitrogen cycling model described by Crise et al. (1998) (hereafter referred to as CCM, 1998) and Crispi et al. (1999) (hereafter referred to as CCM, 1999) is the only work carried out up to now for the

* Corresponding author. Tel.: +90-324-521-2406; fax: +90-324-521-2327.

E-mail address: oguz@ims.metu.edu.tr (T. Oguz).

eastern Mediterranean. It is a simple three-compartment model comprising nitrate as the source of nutrient, phytoplankton and detritus as the living and non-living biological components of the ecosystem. Their model is designed to investigate primarily the role of the circulation on the identification of different oligotrophic regimes of the Mediterranean sub-basins. When compared with the CZCS imagery, the model seems to reproduce observed chlorophyll distributions according to the prevailing cyclonic and anticyclonic flow regimes. One drawback of the model is to neglect the limiting role of the second trophic level on the phytoplankton production. We expect that the absence of phytoplankton–zooplankton interactions may lead to over-prediction of the new production-based phytoplankton biomass and under-prediction of the regenerated production-based biomass.

The present work considers a slightly modified ecosystem model which, in addition to these three compartments, includes zooplankton and ammonium as two other independent state variables. In recent years, five compartment biological models have been accepted as providing the simplest possible representation of pelagic ecosystem tropho-dynamics, and have been applied successfully to different oceanic regimes (e.g., Fasham et al., 1990; McGullicuddy et al., 1995; Doney et al., 1996; McClain et al., 1996; Oguz et al., 1996; Kuhn and Radach, 1997). Here, the model is implemented in its one-dimensional form to the Rhodes and the Ionian basins of the eastern Mediterranean. We consider that the one-dimensional application of the model is an essential prerequisite to understand and quantify the relative roles of different physical and biological processes on the general ecosystem characteristics prior to its three-dimensional basinwide implementation.

The Ionian and Rhodes basins (Fig. 1a,b) are chosen particularly in this study since they reflect two contrasting ecosystems; while the former represents a typical oligotrophic environment, the latter is known to be one of the most productive region of the Mediterranean Sea. These two basins also differ substantially by their dynamical regimes which govern ultimately their ecosystem characteristics. The Ionian Sea, identified as the region from the Sicily Strait to the Cretan passage, is a transition basin across which different water masses (e.g., Modified

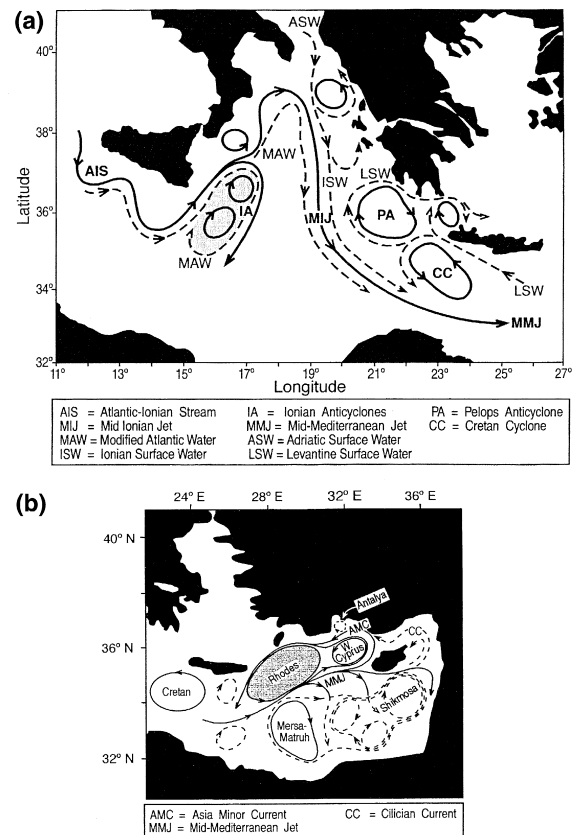


Fig. 1. Schematic diagram of the upper thermocline circulation and water mass pathways in the (a) Ionian basin, (b) Levantine basin. The shaded areas signify the Rhodes and western Ionian gyres.

Atlantic Water, MAW; Levantine Intermediate water, LIW; Eastern Mediterranean Deep Water, EMDW) undergo transformations along their pathways between the eastern and western Mediterranean (Malanotte-Rizzoli et al., 1997). At the near-surface levels which is the most important part of the water column with regard to the biological production, the MAW enters the western Ionian basin advected by the Atlantic Ionian Stream (AIS) which steers northward along the steep topographic slope on the eastern side of Sicily. The AIS jet then bifurcates at $\sim 37^\circ\text{N}$, 17°E into two branches. The first branch turning directly southward encloses multiple centers, forming an overall anticyclonic area in the western Ionian basin. The second AIS branch extends further

into the northeastern Ionian, and then turns southward and crosses the central Ionian basin meridionally as the intense mid-Ionian jet, which finally flows across the Cretan passage as the mid-Mediterranean Jet. A scheme of these circulation features is shown in Fig. 1a. More details and a thorough in-depth analysis of its circulation and water mass characteristics are provided by Malanotte-Rizzoli et al. (1997). The existing information on the biogeochemical characteristics of the Ionian basin is, on the other hand, poor. Rabitti et al. (1994) present some results on the particulate matter and phytoplankton data in the western Ionian basin from the October 1991 survey. Berland et al. (1998) provide the nitrate, phosphate and chlorophyll profiles taken at one station in the same region during July 1983. The eastern Ionian Sea also suffers from lack of detailed measurements. To our knowledge, the water column nutrient and oxygen measurements performed during March–April 1987 and August–September 1987 constitute the only available published data (Souvermezoglou et al., 1992). The pigment data by Antoine et al. (1995) provide supplementary information on the gross primary production characteristics of the Ionian Sea at large.

The physical and chemical characteristics of the Rhodes gyre are reasonably well-explored by a series of systematic surveys of the R.V. Bilim during the last decade (Salihoglu et al., 1990; Ozsoy et al., 1991, 1993; Sur et al., 1993; Ediger and Yilmaz, 1996; Ediger et al., 1999; Lascaratos and Nittis, 1998; Yilmaz and Tugrul, 1999; Yilmaz et al., 1994). It is located in the northern Levantine basin to the west of Cyprus (Fig. 1b), and one of the most persistent cyclonic features of the eastern Mediterranean circulation. It is known as the source area of the Levantine intermediate water mass. Intense and continuous upwelling in the gyre together with winter cooling lead to convective overturning and subsequently dense water mass formation within the upper 400–500 m of the water column, and occasionally down to 1000 m. As we will show here, relatively higher biological production in the Rhodes gyre is associated with its upwelling, mixing and subsequent water mass characteristics. As far as the nutrient and chlorophyll properties are concerned, the data set in the Rhodes gyre region is quite sufficient to calibrate and validate the model results.

The 1989 JGOFS (Joint Global Ocean Flux Study) North Atlantic bloom study reported significant biological variability associated with the eddy features (Robinson et al., 1993). Given the complexity of the upper layer circulation, it is quite reasonable to expect a complex three-dimensional biological structure in the Ionian Sea, too. On one hand, this limits the validity of the one-dimensional model results over the Ionian basin, but on the other hand, it makes the three-dimensional coupled physical–biological model studies quite challenging. In the present study, we restrict our attention only to the western Ionian Sea characterized by the anticyclonic circulation of the AIS and by the least dense upper layer water mass of the Eastern Mediterranean, MAW. It offers therefore completely opposite characteristics to those found in the Rhodes gyre. Moreover, because it is also fully covered by the station network of the October 1991 survey, these data can be used for the verification of the model results. Practically, using a one-dimensional model, we perform here an inter-comparison study to explore the biological characteristics of two regions known qualitatively as the most productive and the most oligotrophic sites of the eastern Mediterranean and to relate them to the prevailing regional physical characteristics. Because of its one-dimensional nature, the role of physical processes governing material transport due to major pathways of the circulation, eddies and gyres as well as of the thermohaline cell can not be investigated with the model.

The paper is organized as follows. A brief description of the model formulation is first provided in Section 2. Its applications to the Rhodes and Ionian basins are then given in Sections 3 and 4, respectively. A discussion of results and conclusions are given in Section 5.

2. Model description

2.1. Model equations

The model is similar to the one described by Oguz et al. (1996) for studying the Black Sea annual plankton dynamics. It is a coupled physical–biological model in which the upper layer dynamical processes are dealt with the one-dimensional form of the

Princeton Ocean Model (Mellor, 1990) including the level 2.5 Mellor and Yamada turbulence parameterization for vertical mixing. The biological state variables considered are phytoplankton biomass P , herbivorous zooplankton biomass H , and labile pelagic detritus D . Nitrate N and ammonium A constitute the other two state variables. The relative roles of nitrogen and phosphate limitations on the eastern Mediterranean ecosystems are presently being explored and will be reported later. For the time being, the same nitrogen limited model will be applied to the Ionian basin. The model therefore should be considered to predict upper limits of the biological production for both basins. When the phosphate limitation is included, they are expected to decrease to some extent.

The local changes of the biological variables are expressed by a time and depth dependent advection–diffusion equation for transport, sources and sinks in a one-dimensional vertical water column. The general form of the equation is given by

$$\frac{\partial X}{\partial t} = \frac{\partial}{\partial z} \left[(K_h + \nu_h) \frac{\partial X}{\partial z} \right] + F_X, \quad (1)$$

where X represents any of the five biological variables, K_h is the vertical eddy diffusion coefficient computed in the model from the Mellor–Yamada level 2.5 turbulence parameterization (see Oguz et al., 1996, for details) and ν_h is its background value, t is time, z is the vertical coordinate, ∂ denotes the partial differentiation. F_X represents the biological interaction terms expressed for the phytoplankton, herbivore, detritus, ammonium, and nitrate equations, respectively, as

$$F_P = \Phi(I, N, A)P - G(P)H - m_p P \quad (2)$$

$$F_H = \gamma G(P)H - m_h H - \mu_h H \quad (3)$$

$$F_D = (1 - \gamma)G(P)H + m_p P + m_h H - \epsilon D + w_s \frac{\partial D}{\partial z} \quad (4)$$

$$F_A = -\Phi_a(I, A)P + \mu_h H + \epsilon D - \Omega A \quad (5)$$

$$F_N = -\Phi_n(I, N)P + \Omega A \quad (6)$$

where the definition of parameters and their values used in the experiments are given in Table 1. The

Table 1
Model parameters used in the numerical experiments

Parameter	Definition	Value	Unit
a	Photosynthesis efficiency parameter	0.01	$\text{m}^2 \text{W}^{-1}$
k_w	Light extinction coefficient for PAR	0.05	m^{-1}
k_c	Phytoplankton self-shading coefficient	0.04	$\text{m}^2 (\text{mmol N})^{-1}$
σ_p	Maximum phytoplankton growth rate	1.5	day^{-1}
m_p	Phytoplankton mortality rate	0.04	day^{-1}
σ_g	Zooplankton maximum grazing rate	0.6	day^{-1}
m_h	Zooplankton mortality rate	0.04	day^{-1}
μ_h	Zooplankton excretion rate	0.07	day^{-1}
γ_h	Food assimilation efficiency	0.75	Dimensionless
R_n	Half saturation constant in nitrate uptake	0.5	mmol N m^{-3}
R_a	Half saturation constant in ammonium uptake	0.2	mmol N m^{-3}
R_g	Half saturation constant for zooplankton grazing	0.5	mmol N m^{-3}
ψ	Ammonium inhibition parameter of nitrate uptake	3	$(\text{mmol N m}^{-3})^{-1}$
ϵ	Detritus decomposition rate	0.1	day^{-1}
w_s	Detrital sinking rate	8.0	m day^{-1}
Ω_a	Nitrification rate	0.05	day^{-1}
ν_b	Background kinematic diffusivity	0.1	$\text{cm}^2 \text{s}^{-1}$

functions $\Phi(I, N, A)$ and $G(P)$ denote the light and nutrient limited phytoplankton growth and zooplankton grazing rates, respectively. The latter is represented by the maximum ingestion rate σ_g multiplied by the Michaelis–Menten type limitation function

$$G(P) = \sigma_g \frac{P}{R_g + P} \quad (7)$$

where R_g is the half saturation constant for the zooplankton grazing. Eq. (7) implies that zooplankton grazes only on phytoplankton. Their grazing on the detrital material is not taken into account since this usually constitutes only a small fraction of zooplankton diet (about 10%).

The phytoplankton production is parameterized as product of the maximum growth rate σ_m , minimum of the light and nutrient limitation functions and the phytoplankton standing stock. The temperature limitation of the phytoplankton growth is not included in the model, for simplicity. Thus, the net growth rate $\Phi(I, N, A)$ is given by

$$\Phi(I, N, A) = \sigma_m \min[\alpha(I), \beta_t(N, A)] \quad (8)$$

where min refers to the minimum of either the light limitation function $\alpha(I)$ or the total nitrogen limitation function $\beta_t(N, A)$. The latter is expressed as the sum of ammonium and nitrate limitation functions, $\beta_a(A)$ and $\beta_n(N)$, respectively

$$\beta_t(N, A) = \beta_n(N) + \beta_a(A). \quad (9)$$

They are given by the Michaelis–Menten type uptake formulation as

$$\beta_a(A) = \frac{A}{R_a + A},$$

$$\beta_n(N) = \frac{N}{R_n + N} \exp(-\psi A), \quad (10)$$

where R_n and R_a are the half-saturation constants for nitrate and ammonium uptake, respectively. The exponential term in Eq. (10) represents the inhibiting effect of ammonium on nitrate uptake, with ψ signifying the inhibition parameter.

The individual contributions of the nitrate and ammonium uptakes, respectively, to the phytoplankton production, given in Eqs. (5) and (6), are represented by

$$\Phi_n(I, N) = \Phi(I, N, A) \left(\frac{\beta_n}{\beta_t} \right),$$

$$\Phi_a(I, A) = \Phi(I, N, A) \left(\frac{\beta_a}{\beta_t} \right). \quad (11)$$

The light limitation is parameterized according to the hyperbolic tangent function of Jassby and Platt (1976) and exponentially decaying irradiance with depth,

$$\alpha(I) = \tanh[aI(z, t)] \quad (12)$$

$$I(z, t) = I_s \exp[-(k_w + k_c P)z], \quad (13)$$

where a denotes photosynthesis efficiency parameter controlling the slope of the $\alpha(I)$ vs. irradiance curve

at low values of the photosynthetically active radiance (PAR). I_s denotes the surface intensity of PAR taken as the half of the climatological incoming solar radiation. k_w is the light attenuation coefficient of sea water, and k_c is the phytoplankton self-shading coefficient. In the above formulation, k_w and k_c are taken to be constant with depth. The daily variation of the light irradiance, and hence of the phytoplankton growth, are neglected since the biological processes we consider have time scales much longer than a day.

Eq. (2) implies that the variations of phytoplankton stock are governed by a balance between primary production and losses due to herbivore grazing and mortality. A certain fraction of the food grazed by herbivores is ingested [represented by the first term in Eq. (3)] and the rest is egested as fecal pellets to the detrital pool [the first term in Eq. (4)]. The mortality and excretion are two forms of herbivore losses from the system [the second and third terms of Eq. (3)]. The dead planktonic material [the second and third terms of Eq. (4)] constitutes an additional detritus source. It sinks with a speed w_s and, at the same time, is remineralized and converted to ammonium. These two processes are represented by the last two terms in Eq. (4). The zooplankton excretion and remineralization of detritus form the ammonium sources. Ammonium is consumed in the phytoplankton growth and converted to nitrate by the nitrification process. The nitrate Eq. (6) represents a balance between nitrate input through the nitrogen recycling mechanism and its consumption in the phytoplankton growth.

2.2. Boundary conditions

No-flux conditions described by

$$(K_h + \nu_h) \frac{\partial X}{\partial z} = 0 \quad (14)$$

are specified both at the surface and the bottom boundaries of the model for the variables $X = P, H, N,$ and A . For detritus, it is modified to include the contribution of downward sinking flux

$$(K_h + \nu_h) \frac{\partial D}{\partial z} + w_s D = 0. \quad (15)$$

The bottom boundary of the model is taken at the 400 m depth for the Rhodes case and at the 300 m depth for the Ionian case, which are well below the euphotic zone comprising only the upper 100 m of the water column. Considering our choice of moderate detritus sinking rates (see Table 1), the advantage of locating the bottom boundary at considerable distance away from the euphotic layer is to allow complete remineralization of the detrital material until it reaches the lower boundary of the model. This approach avoids prescription of the non-zero flux boundary condition in order to compensate the loss of detritus (if any) to the deep interior from the boundary. The assumption of complete mineralization is introduced here as a convenience. Within the framework of one-dimensional model, if it is relaxed, particulate matter export flux to deeper parts of the sea must be compensated by influx of nitrate at the base of the model at each time step. This is almost identical with converting all particulate matter into nitrate form within the lower part of the water column. In three-dimensional case, the situation is different and particulate matter loss may be compensated by lateral fluxes. The complete remineralization was ensured by setting appropriate decomposition and sinking rates of detrital material in the model. We note that Eqs. (2)–(6) together with the boundary conditions (14) and (15) provide a closed, fully conserved system. The state of the system at time t is governed solely by internal dynamical processes without any contribution from external sources.

The physical model is forced by daily climatological atmospheric fluxes. The wind stress data are taken from the ECMWF climatology. The heat flux data are provided by May (1982) whereas the data given by Antoine et al. (1995) for the Ionian Sea are used for the specification of PAR for both simulations. The heat flux data, however, are adjusted slightly to provide the zero annual mean over the year, even though this net zero balance may be in contradiction with the actual negative heat budget measured for the entire Mediterranean as well as for its western and eastern sub-basins. This adjustment is however necessary to avoid the drift of the model from its perpetual state due to continuous warming/cooling of the water column during the time integration of the temperature equation. The

resulting adjusted heat flux distributions over the year are shown in Fig. 2. Winter cooling is greater ($\sim 200 \text{ W/m}^2$) in the Rhodes basin as compared to the value of 130 W/m^2 for the Ionian Sea. In the summer, the warming in the Rhodes basin reaches 180 W/m^2 which is also higher than that of the Ionian basin by about 40 W/m^2 . The mean daily PAR attains its maximum intensity of 140 W/m^2 during the summer months, whereas its minimum value is set to 40 W/m^2 during December and January. Instead of prescribing the fresh water flux at the surface, the model is forced by the surface salinity whose annual variations are specified by the Mediterranean Oceanic Data Base (MODB) data set (Brasseur et al., 1996). The forcing by surface salinity instead of the fresh water flux using evaporation minus precipitation data is a matter of convenience here since it provides more realistic yearly salinity variations in the near-surface levels of the water column.

Although the atmospheric forcing functions used in the model are rather idealized, they are adequate for the purpose of the present work since the surface layer dynamics is introduced into the biological model only indirectly by specification of the vertical eddy diffusivity. There is no other feedback mechanism between the physical and biological models.

2.3. Initial conditions

The model is initialized with the stably stratified upper ocean temperature and salinity profiles representative of the summer/autumn climatological conditions (Fig. 3a). The same initial temperature profile

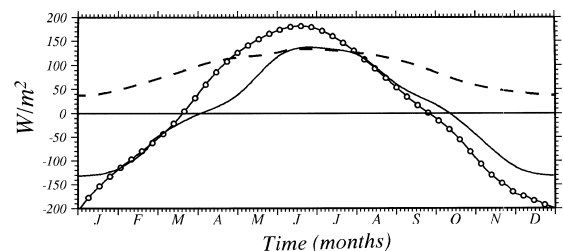


Fig. 2. Climatological daily averaged heat fluxes (in W m^{-2}) for the Ionian basin (continuous line) and the Rhodes basin (continuous line with open circles), and photosynthetically available radiation flux (in W m^{-2}) (broken line) used in the simulations.

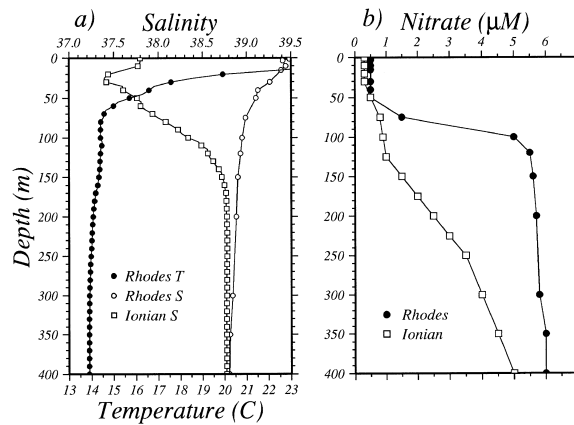


Fig. 3. The profiles of (a) temperature and salinity, and (b) nitrate used for the model initialization.

is used for both Rhodes and Ionian simulations since the subsurface structures of these two regions reflect characteristics of the LIW below 100–150 m depth. The salinity, on the other side, differs greatly between these two basins. The upper 150 m of the water column in the Rhodes gyre is occupied by much more saline water mass (with $S > 39.0$ ppt) as compared to less saline modified Atlantic-based waters (minimum $S \sim 37.4$ ppt) in the western Ionian basin (Fig. 3a). In the biological model, the initial nitrate amount drives the system as it is entrained and diffused upward and utilized ultimately for the biological production. In the absence of any external source and sink as implied by the boundary conditions (see Eqs. 14 and 15), the model simply redistributes the initial nitrogen source among the living and nonliving components of the system. Thus, specification of the initial phytoplankton, zooplankton, detritus and ammonium distributions is unimportant as they will be generated by the model during its transient evolution. The initial subsurface nitrate structure however will govern, to a large extent, the level of productivity in the euphotic zone. Accordingly, the state variables except nitrate are initialized by a vertically uniform small, non-zero value within the euphotic layer for both cases. The initial vertical nitrate structures are specified according to the data given by Berland et al. (1998) and Yilmaz and Tugrul (1999). These observed profiles, shown in Fig. 3b, demonstrate clearly that these two basins differ substantially in terms of their subsurface nitrate structure below the 100 m depth. The Rhodes

gyre reveals vertically uniform subsurface nitrate concentrations in the order of $5 \mu\text{M}$. On the other side, the western Ionian subsurface nitrate concentrations increase gradually with depth and reach the similar nitrate level of the Rhodes basin only below 500 m depth. As it will be presented in the following sections, these differences in the nitrate and salinity structures play a crucial role on the ultimate biological characteristics of these two regions.

2.4. Numerical procedure

The model equations are solved using the finite difference procedure described in Mellor (1990). A total of 51 vertical levels is used to resolve water column. The grid spacing is compressed slightly towards the surface to increase the resolution within the euphotic zone. Accordingly, the vertical grid spacing is at most 10 m for the Rhodes case and about 7 m for the Ionian case. This resolution is found to be quite adequate to represent properly steep gradients of density and nitrate between the seasonal thermocline/pycnocline and the base of the euphotic zone. The numerical scheme is implicit to avoid computational instabilities due to small grid spacing and fully documented in Mellor (1990). A time step of 5 min, used in the numerical integration of the equations, provides a stable solution without introducing numerical noise.

First, the physical model is integrated for 5 years. An equilibrium state with repeated yearly cycle of the dynamics is achieved after 3 years of integration

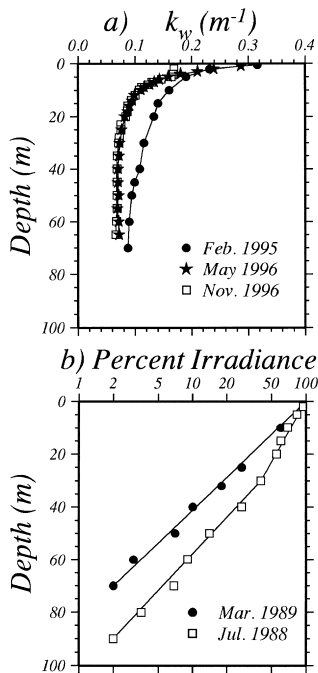


Fig. 4. (a) The profiles of extinction coefficients (in m^{-1}) obtained by the measurements in the Rhodes gyre region during February 1995, May and November 1996, (b) variation of percentage light intensity with depth in the Rhodes cyclonic region during July 1988 (open squares) and March 1989 (solid circles) (after Yilmaz et al., 1994).

in response to the external forcings and to the internal processes in the system. Using the results of the fifth year of the physical model, the biological model is then integrated for 4 years to obtain repetitive annual cycles of the biological variables. The results of the biological model presented here are based on the fourth year of integration.

2.5. Choice of the parameters

The parameters used in the simulations are chosen from the available data and literature related to the Mediterranean ecosystem modeling (e.g., Andersen and Nival, 1988; Oguz et al., 1996; Crise et al., 1998; Levy et al., 1998) and then adjusted to reproduce major observed features of the systems through a series of sensitivity studies. For the Rhodes simulations, the values of extinction coefficients (k_w , k_c) are chosen on the basis of the light measurements carried out in the region during different seasons

(Ediger et al., 1999). The data from the February 1995, May 1996 and November 1996 surveys (Fig. 4a) suggest strong variations of the extinction coefficient within the upper 20 m followed by rather uniform values at deeper levels (between 0.05 and 0.1 m^{-1}). The data from July 1988 and March 1989 (Fig. 4b) also reveal quite similar variations of the extinction coefficient with the values of 0.046 m^{-1} for the former and 0.054 m^{-1} for the latter data. Thus, we set $k_w = 0.05 m^{-1}$ which reveals the position of the one percent light level at 95 m depth (Fig. 5). The increase in the near-surface values is incorporated by setting $k_c = 0.04 m^{-1}$. This choice increases the total extinction coefficient to about 0.15–0.20 m^{-1} during the spring bloom period, with the corresponding shallowest position of the euphotic zone depth at 25 m (Fig. 5).

The phytoplankton parameters are chosen typically for diatoms; 1.5 day^{-1} for the maximum growth rate, 0.04 day^{-1} for the overall contribution of natural mortality and excretion. The parameters for the herbivores are adjusted according to mesozooplankton physiological parameters. Hence, the maximum grazing, mortality and excretion rates are taken as 0.6, 0.04 and 0.04 day^{-1} , respectively. The detritus breakdown rate is 0.1 day^{-1} being more appropriate for the small-to-moderate size particles sinking with a constant rate of 10 $m day^{-1}$. The nitrification rate is 0.05 day^{-1} . Assumption of constant nitrification rate is more appropriate for the deeper part of the water column. In the euphotic zone, nitrification is light limited, and does not play a major role. As will be shown in Fig. 13, our simulations which indicate only 30% of nitrification taking place within the euphotic zone are therefore consistent with the ob-

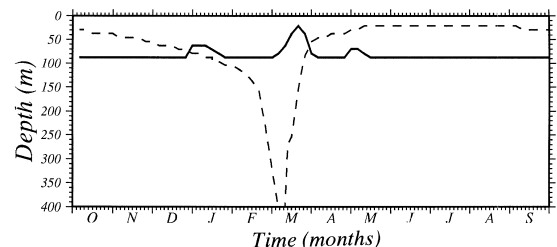


Fig. 5. Simulated annual cycles of the mixed layer depth (broken line) and the euphotic zone depth (continuous line) in the Rhodes basin.

servations. A list of these parameters together with the values assigned to them in the standard Rhodes and Ionian experiments are given in Table 1.

3. Simulation of Rhodes basin ecosystem

3.1. Stratification characteristics

The annual variations of the temperature and σ_t for the upper 150 m of the water column are shown in Fig. 6a,b. The temperature structure (Fig. 6a) exhibits all the major features of the observed variations in the Rhodes gyre during the summer and winter months. Starting with the autumn season, the water column begins to cool gradually and, at the

same time, homogenizes to greater depths as a result of convective overturning induced by the atmospheric cooling shown in Fig. 2. At the end of January, the mixed layer water temperature is about 14.5–15.0°C and the mixed layer depth is about 100 m. In February, the temperature attains its lowest value of about 14.3°C, and the mixed layer homogenizes throughout the water column of 400 m taken as the lower limit of the model. The corresponding density of this water mass is 29.19 kg/m³ (Fig. 6b) which, together with the temperature, represent typical characteristics of the LIW known to be formed in the gyre during the winter months (Ozsoy et al., 1993; Sur et al., 1993). With our idealized atmospheric forcing (cf. Fig. 2), cooling of the water column continues until mid-March after which the

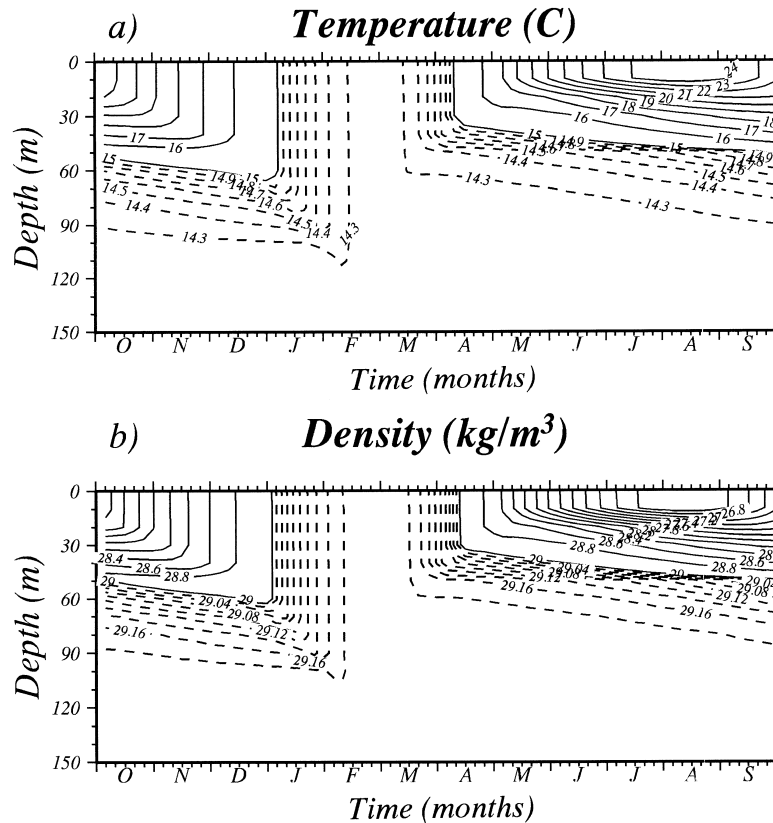


Fig. 6. Simulated annual distributions of (a) temperature and (b) density within the upper 150 m depth of the water column in the Rhodes basin. For temperature, contours with continuous lines are at intervals of 1°C, and with broken lines at 0.1°C. For density, contours with continuous lines are at intervals of 0.2 kg/m³, and with broken lines at 0.02 kg/m³. In both plots the time axis starts at October 1 and ends at September 30.

warming period starts and the seasonal thermocline begins to establish during spring and summer months. The surface temperature increases up to 24.5°C dur-

ing August, the corresponding density value is about 26.5 kg/m³. The seasonal thermocline is located at its shallowest position of 15–20 m depth during this

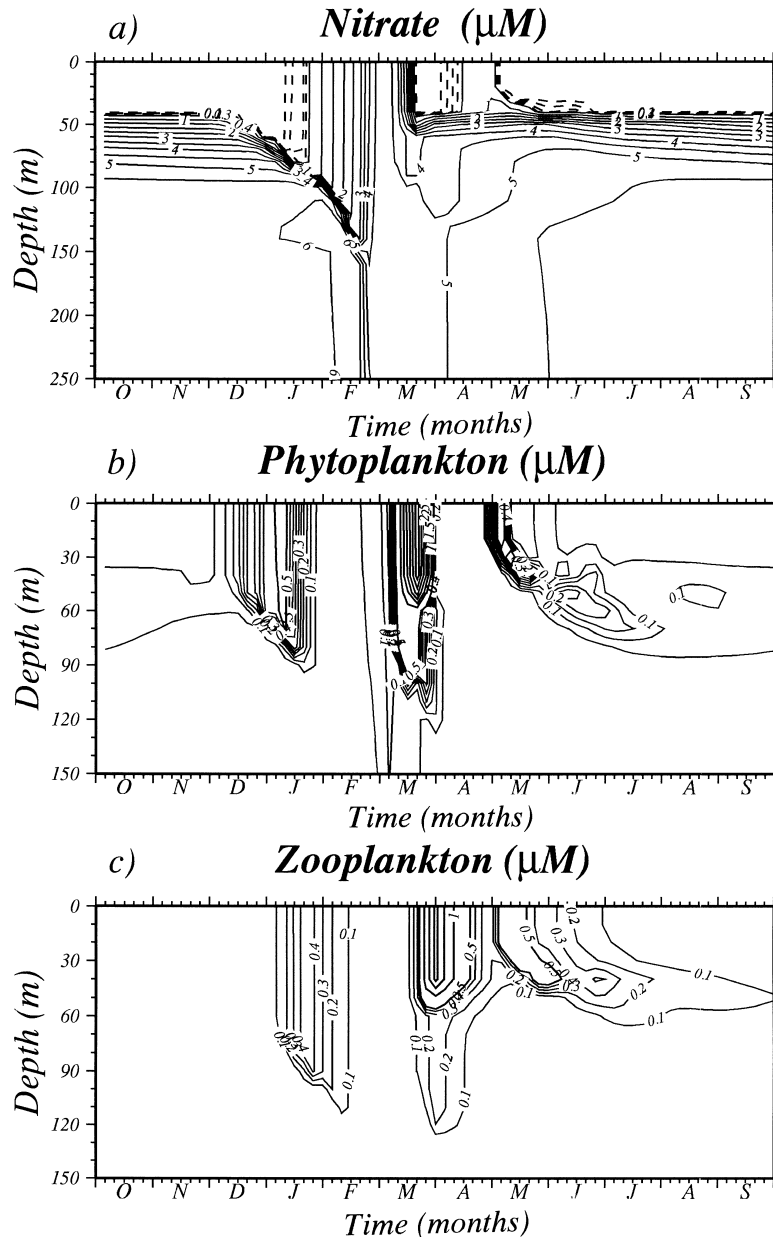


Fig. 7. Simulated annual distributions of (a) nitrate, (b) phytoplankton, (c) zooplankton, (d) detritus, (e) ammonium, within the upper 150 m depth for phyto- and zooplankton and the upper 250 m depth for others in the Rhodes basin. Units are in mmol N m^{-3} . For nitrate, continuous lines are contours at intervals of 0.5 mmol N m^{-3} and broken lines at intervals of 0.1 mmol N m^{-3} . In all plots, the time axis starts at October 1 and ends at September 30.

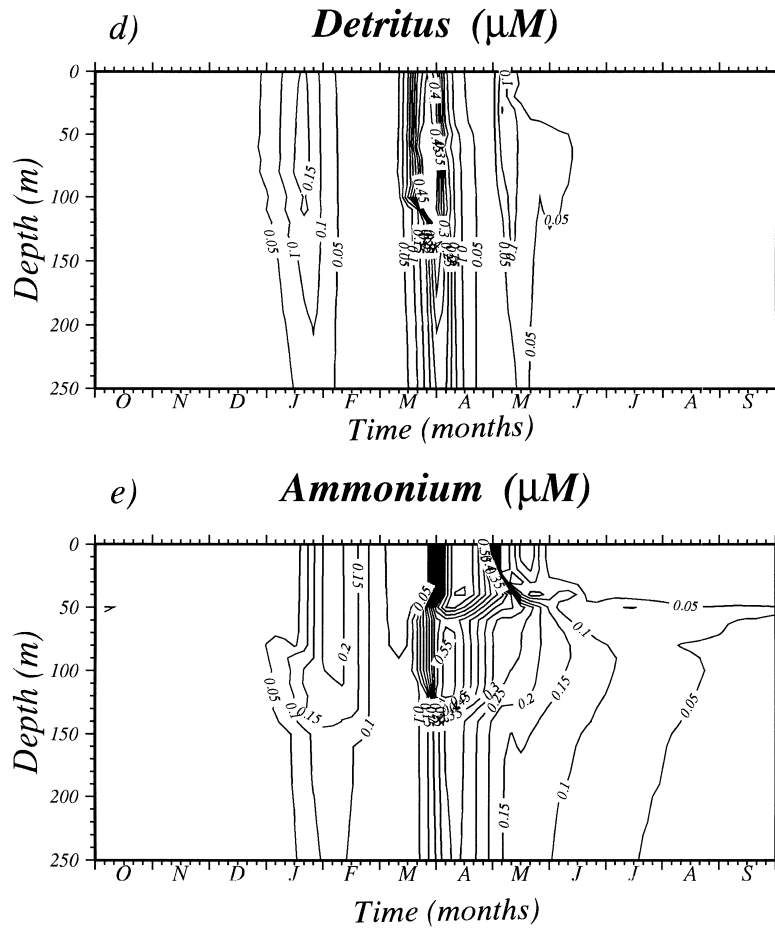


Fig. 7 (continued).

period. Thus, the mixed layer in the model changes over a depth range between 20 m and 400 m, as shown in Fig. 5. The seasonal thermocline is followed by a 50 m thick highly stratified zone across which the temperature decreases below 15.0°C , whereas the density increases to more than 29.1 kg/m^3 . This represents typical characteristics of the LIW in this region.

The annual temperature and density distributions shown in Fig. 6a,b agree fairly well with the observations presented in Ozsoy et al. (1991, 1993). We note that reproduction of such highly variable thermohaline structure is largely due to the implementation of a fairly sophisticated turbulence parameterization in the model. The same approach used in our previous modeling studies in the Black Sea (Oguz et

al., 1996, 1998) and the Adriatic Sea (Bergamasco et al., 1999) also reproduced successfully the dense water mass formation and related thermohaline characteristics for these basins. A similar three-dimensional application to the intermediate water mass formation and spreading in the Levantine Sea is reported by Lascaratos and Nittis (1998).

3.2. Annual ecosystem dynamics

In agreement with its vertical mixing and stratification characteristics, the nitrate structure undergoes considerable variations during the year (Fig. 7a). During the entire summer and autumn seasons, the mixed layer is extremely poor in nutrients with nitrate concentrations of about 0.1 mmol/m^3 . The

nitrate depletion arises due to lack of supply from the subsurface levels because of the presence of a strong seasonal thermocline/pycnocline. The zone of high stratification below the seasonal thermocline (cf. Fig. 6a,b) coincides with the strong nitrate variations (the so-called nitracline). Approximately below 80–90 m depths, nitrate attains its typical deep water concentrations more than 5.0 mmol/m^3 . This structure undergoes substantial modification during the winter months as the convective overturning mechanism brings the nitrate-rich subsurface waters to near-surface levels. Under such conditions, nitrate concentrations attain their maximum values of 4.5 mmol/m^3 over the 400 m deep homogeneous water column in February.

The phytoplankton exhibits a major algae production during the first half of March (Fig. 7b) immediately after the shallowing of the mixed layer (cf. Fig. 5) and higher flux of solar irradiance (cf. Fig. 2) penetrating to deeper levels. Since the water column was already replenished by nitrate, all these conditions favor a phytoplankton bloom, shown in Fig. 7b as an exponential increase of algae concentrations during the second week of March. The high nitrate concentrations, built up in the water column during the winter, lead to a very intense bloom with maximum biomass of about 3.8 mmol N/m^3 . It extends to the depth of 120 m, but its major part is confined to the upper 65 m because of the increasing role of self-shading on the light limitation. Following a week-long intense period, the bloom weakens gradually within the last week of March and terminates completely by the end of that month.

The early spring phytoplankton bloom initiates other biological processes within the living and non-living components of the pelagic ecosystem. Soon after the termination of the phytoplankton bloom, mesozooplankton biomass increases up to 2.2 mmol N/m^3 during April (Fig. 7c). This period also coincides with increased detritus and ammonium concentrations (Fig. 7d,e) supplied by excretion and mortality of phytoplankton and mesozooplankton communities. The major detritus accumulation in the water column in fact proceeds the termination of phytoplankton bloom at beginning of April.

The role of remineralization responsible for transforming the particulate organic nitrogen to inorganic dissolved nitrogen is indicated by increased ammo-

nium concentrations up to 0.7 mmol N/m^3 in March–April period in Fig. 7e. Its eventual oxidation due to nitrification process leads to nitrate accumulation in the mixed layer and nitracline, and causes a short-term increase in phytoplankton biomass up to about 0.5 mmol N/m^3 within the mixed layer during the first half of May (Fig. 7b). This secondary bloom is also followed by a small increase in mesozooplankton biomass, as well as in detritus and ammonium concentrations. The phytoplankton bloom continues below the seasonal thermocline for another month by consuming available nitrate and ammonium within the nitracline zone. The subsurface biomass diminishes gradually towards the end of July as the losses due to mesozooplankton grazing and phytoplankton mortality exceeds production.

The phytoplankton exhibits another weak bloom from mid-December to mid-January. This is associated with the consumption of nitrate which is made readily available by the convective mixing initiated in the water column with the beginning of cooling season. Once again, it is followed by increase in mesozooplankton stocks in January–February.

We do not intend here to present a detailed sensitivity study with a series of model solutions corresponding to different choices of parameters, since no detailed observations are available to assess realism of these solutions. However, it is interesting to show the role of the strength of atmospheric cooling on the phytoplankton production since this directly affects the intensity of vertical mixing in the winter months. We have therefore repeated the Rhodes simulation by halving the heat flux over the entire year, and thus reducing the maximum cooling to 100 W/m^2 . The comparison of the euphotic-zone averaged total nitrogen concentration and phytoplankton biomass with those of the previous case is shown in Fig. 8. As expected, the reduced cooling results in weaker vertical mixing in the water column and hence a shallower mixed layer and weaker entrainment. The mixed-layer deepening is now limited to the upper 150 m depth. The maximum nitrogen concentration in the euphotic zone prior to the March bloom is reduced from 5 mmol N/m^3 in the previous case to about 3 mmol N/m^3 (Fig. 8a), giving rise to a weaker early-spring phytoplankton bloom confined more towards the free surface. The euphotic zone averaged phytoplankton biomass decreases from ~

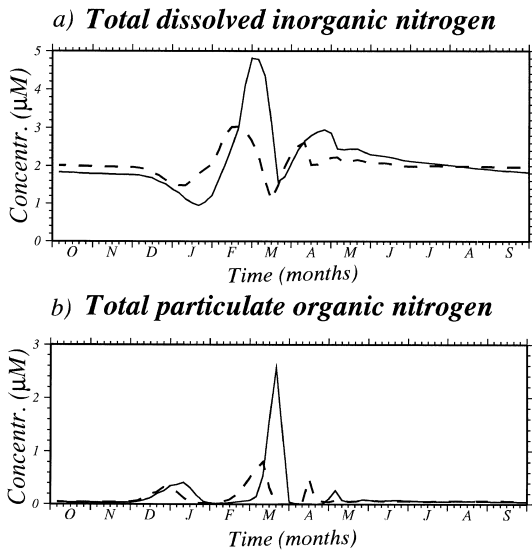


Fig. 8. Simulated annual distributions of (a) total dissolved inorganic nitrogen, and (b) total particulate organic nitrogen averaged over the upper 100 m depth of the water column in the Rhodes basin. The continuous line represent the solutions for the standard run and the broken lines for the model experiment with weaker heat flux forcing. The time axis starts at October 1 and ends at September 30.

2.5 mmol N/m³ of the previous case to ~ 0.8 mmol N/m³ (Fig. 8b). As pointed out before, the reduced mixing also causes an earlier development of the bloom by about 12 days. These results point to possible interannual variabilities of the intensity of the phytoplankton bloom due to different winter atmospheric conditions. Milder and warmer winters should tend to generate earlier and weaker phytoplankton blooms.

3.3. Model-data comparison

Expressing phytoplankton biomass in terms of chlorophyll *a* concentrations requires to specify the values of carbon to chlorophyll (C:Chl) and the carbon to nitrogen (C:N) ratios. Following the data provided by Ediger et al. (1999), we take C:N = 12 as a representative value for the entire euphotic zone. The C:Chl values, on the other hand, vary between 50 and 100, apart from some high values near the surface. We accept C:Chl = 75 as water column representative value. Using these conversion rates, 1 mmol N/m³ phytoplankton biomass corresponds to

1.6 mg Chl/m³ chlorophyll *a*. Recently, there have been several attempts to compute these ratios from models through empirically based algebraic relations expressed in terms of light and nutrient limitations (e.g., Doney et al., 1996; Levy et al., 1998; CCM, 1998). At this stage of our modeling efforts, however, we do not see the advantage of using such relations for the eastern Mediterranean before they are verified by specific observations.

Unfortunately, no detailed in-situ time series data on the model variables are available in the Rhodes area, and in more general terms in the whole eastern Mediterranean. The model-data intercomparison can therefore be based only on general characteristics of the ecosystem in a rather qualitative way. Fig. 9 shows observed chlorophyll and nitrate profiles from the Rhodes gyre region for the winter, summer and autumn seasons, respectively. The March 1992 profiles represent vertically uniform conditions of intense mixing with nitrate and chlorophyll concentrations of about 5.0 mmol N/m³ (Fig. 9a) and 0.4 mg Chl/m³ (Fig. 9b). As it was indicated before they represent typical conditions prior to the early spring bloom. The corresponding total particulate organic nitrogen (PON) data (Fig. 10a) also shows a small but vertically uniform structure, which is also provided by the model (Fig. 10b). The March 1994 profile, on the other hand, reveals nitrate depletion in the surface mixed layer of about 30 m followed by a broad transition zone up to the base of the euphotic layer. Similarly, a low chlorophyll concentration of about 0.2 mg Chl/m³ inside the mixed layer in-

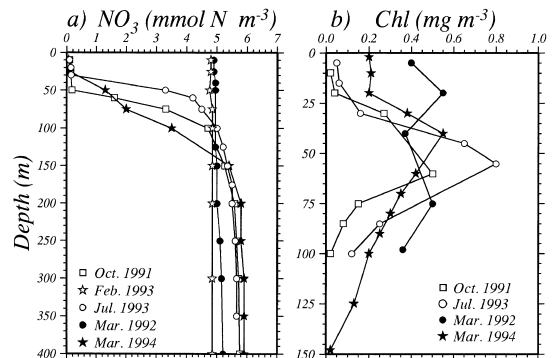


Fig. 9. Vertical profiles of (a) nitrate (after Yilmaz and Tugrul, 1999) and (b) chlorophyll *a* (after Ediger et al., 1999) in the Rhodes gyre at different periods.

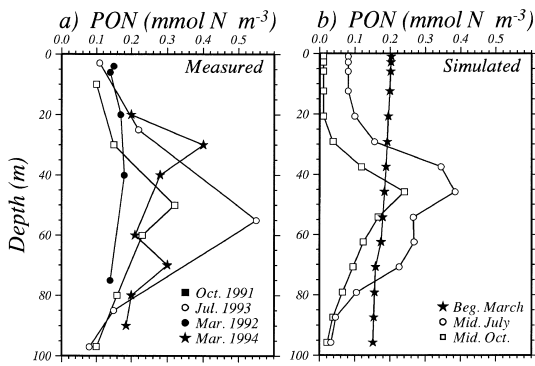


Fig. 10. Vertical profiles of PON in the Rhodes gyre (a) measured during October 1991 (solid squares), March 1992 (solid circles), July 1993 (open circles) and March 1994 (solid stars) (after Ediger et al., 1999), and (b) simulated at the same periods of the model year.

creases linearly to 0.6 mg Chl/m^3 at the depth of 60 m, and then decreases linearly again towards the base of the euphotic zone. The slight slope of the nitracline in Fig. 9a suggests the presence of nitrogen recycling below the seasonal thermocline, consistent with the subsurface chlorophyll maximum layer shown in the corresponding chlorophyll profile in Fig. 9b. The form of these profiles reflects typical post-bloom conditions. If that is really the case, this bloom should then take place in early February 1994 instead of early March as simulated by the model. Considering the fact that winter 1994 was one of the mild winters of recent years this could be a real possibility. The July and October chlorophyll *a* profiles (Fig. 9b) indicate a subsurface maximum around 60 m depth with concentrations of about 0.8 and 0.5 mg Chl/m^3 , respectively. The presence of this subsurface layer is also supported by the PON data (Fig. 10a) which also yields similar maxima at the same levels. Observation of noticeable subsurface chlorophyll-*a* concentrations during October implies the continuation of the summer subsurface production until the development of the early winter bloom at the end of the year. The deep chlorophyll maximum (DCM) layer and its variations during the year are in fact better shown in Fig. 11 which is based on the data from 23 stations in the Rhodes gyre area visited by R.V. Bilim during the 1986–1995 period. According to this figure, the DCM values seem to remain at a steady level between 0.3 and 0.5 mg Chl/m^3

Chl/m^3 during the summer and autumn period. The winter and early spring values, on the other hand, represent the mixed layer average quantities since the DCM layer has not yet developed at that time of the year. Here, the most noticeable feature is the chlorophyll value of 3.0 mg Chl/m^3 shown in March. This data confirm our simulation of the strong early spring bloom in this region.

The nitrate profiles (Fig. 9a) exhibit nitrate depletion in the mixed layer followed by strong variations across the nitracline. The model can predict this layer during June after which the model subsurface chlorophyll concentrations fall to the oligotrophic limit of 0.15 mg Chl/m^3 . This feature is however a known deficiency of single compartment aggregated plankton models. As shown by Oguz et al. (1998, 1999), introducing size fractionation into the planktonic groups leads to prediction of stronger and longer-lasting subsurface chlorophyll *a* concentrations since more than one group of prey-predator interactions are allowed in the model ecosystem.

According to the data given by Antoine et al. (1995) for the northern Levantine Sea, the monthly mean CZCS-derived sea surface chlorophyll values in the January–March period are comparable or even smaller than the corresponding values of the summer months. The annual mean of the data, $0.08 \pm 0.04 \text{ mg Chl/m}^3$, was in fact very small value. The absence of relatively high surface chlorophyll values in the winter months, and particularly for March in the CZCS data is striking and contradicts our model results. This has led us to re-examine the Level 1 daily CZCS data provided for 1979–1985 period by the Joint Research Centre of the European Commission in Ispra, Italy. The region was very poorly

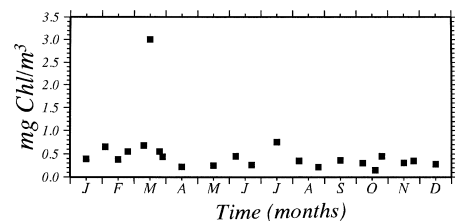


Fig. 11. A composite picture of the yearly euphotic layer average chlorophyll concentration distribution in the Rhodes basin (in mg Chl/m^3). The data compiled from the measurements of R.V. Bilim during 1986–1995 period (after Ediger, 1995).

covered as we found only 149 daily images within the entire data set. A documentation of the data according to the months of the years 1979–1985 is given in Table 2.

The majority of the CZCS data set for the northern Levantine covers the summer and autumn months. The 112 images of the total 149 reveal surface chlorophyll values below the detection limit of 0.05 mg Chl/m³ for the entire May–November period. They therefore indicate absence of any phytoplankton growth inside the mixed layer for this period in this region. Twelve images are available for March, 6 of them cover March 12–30, 1980 period in which the chlorophyll values lie within the 0.3–0.5 mg Chl/m³ range, suggesting that the bloom probably took place earlier in this particular year. Four other images which are also from the last 10 days of March yield similar values without any bloom signature. The only image which is able to capture the relatively strong chlorophyll concentrations is the one taken at March 15, 1985 (Fig. 12a). It provides a clear evidence of a patchy phytoplankton bloom event only inside the Rhodes gyre whereas the Mersa Matruh anticyclonic gyre on its southern part is characterized by very low (0.05 mg Chl/m³) surface chlorophyll values. The next available image of 10 April 1985 (Fig. 12b) shows continuation of the bloom in the Rhodes region although the image can display only the periphery of the gyre because of cloud coverage on the rest of the Levantine basin. Furthermore, only few images are available for January and February. Among them the images from February 2 and 18, 1979 show an increase in the chlorophyll concentrations from 0.5 to about 1.0 mg/m³ during this period, thus, implying an initiation of the early spring bloom in the region.

Table 2
Documentation of daily CZCS images for the Rhodes basin

Year	Jan	Feb	Mar	Apr	May	Jun	Jul	Aug	Sep	Oct	Nov	Dec
1979	1	2	1	3	4	–	5	–	4	1	1	1
1980	–	–	6	2	1	9	7	4	1	2	3	1
1981	–	1	–	1	2	1	7	5	5	5	5	2
1982	3	–	1	3	2	1	2	11	3	4	1	2
1983	1	–	1	–	2	4	1	1	2	1	1	–
1984	–	–	1	–	–	–	–	1	–	1	1	1
1985	–	–	1	2	–	–	–	1	–	1	–	–
total	5	3	11	11	11	15	22	22	15	15	12	7

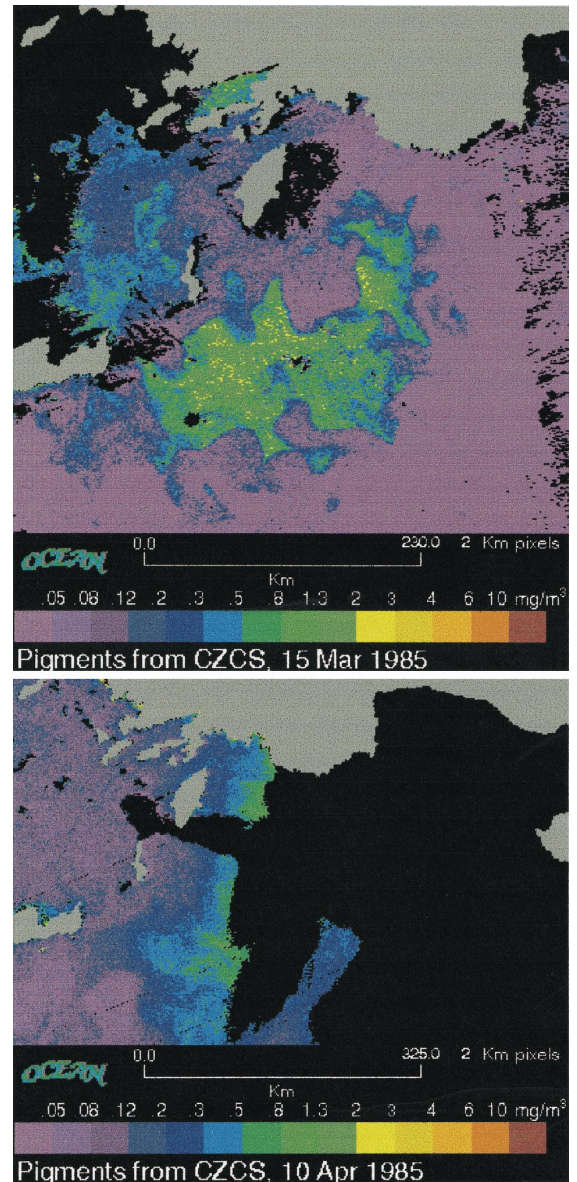


Fig. 12. The CZCS images for March 15 and April 10, 1985. The images are provided by V. Barale from the Marine Environment Unit of Space Application Institute at the Joint Research Center of the European Commission in Ispra, Italy.

3.4. Annual plankton budget and primary production estimates

The annual mean intercompartmental transfer rates within the euphotic zone and the vertical fluxes

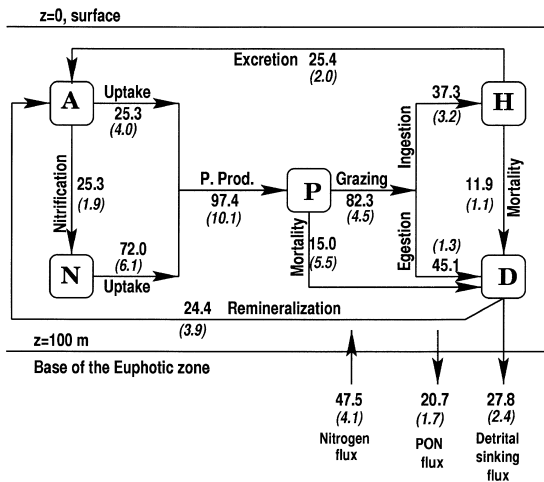


Fig. 13. The annual nitrogen budget (in $1 \text{ g C m}^{-2} \text{ yr}^{-1}$) in the euphotic zone for both Rhodes and Ionian simulations. The Ionian budget is shown by the numbers in parentheses.

across its base are shown in Fig. 13. They are expressed in units of $\text{g C m}^{-2} \text{ yr}^{-1}$ and obtained by converting all the fluxes using $1 \text{ mmol N} \cong 80 \text{ mg C}$. At the base of the euphotic zone, the budget implies that the vertical diffusive nitrogen (nitrate + ammonium) flux of $47.5 \text{ g C m}^{-2} \text{ yr}^{-1}$ from below is balanced by the sum of downward PON flux of $20.7 \text{ g C m}^{-2} \text{ yr}^{-1}$ due to turbulent mixing and detrital sinking flux of $27.8 \text{ g C m}^{-2} \text{ yr}^{-1}$ leaving the euphotic zone. The total primary production (PP) is estimated as $97.4 \text{ g C m}^{-2} \text{ yr}^{-1}$, 25% of which is met by ammonium uptake and the rest by nitrate uptake. We note, however, that only two-third of the overall nitrate uptake of $72.0 \text{ g C m}^{-2} \text{ yr}^{-1}$ is supported from the subsurface levels and represents really new production, the rest is accounted by the recycling mechanism within the euphotic zone. The budget suggests approximately 40% of the PP ($37.3 \text{ g C m}^{-2} \text{ yr}^{-1}$) is utilized for the secondary production, whereas the rest goes directly into the detrital pool.

The PP estimation of $97.4 \text{ g C m}^{-2} \text{ yr}^{-1}$ agrees fairly well with the value of $86.8 \text{ g C m}^{-2} \text{ yr}^{-1}$ computed by Antoine et al. (1995) on the basis of the CZCS analyses for the Northern Levantine. Using the data from 1986 and 1987 surveys of R.V. Bilim, Salihoglu et al. (1990) suggested a lower value of $60 \text{ g C m}^{-2} \text{ yr}^{-1}$. This estimate, however, does not

cover the data from productive spring period, and therefore underestimates the annual rate. Our estimate is also comparable with the value of $105 \text{ g C m}^{-2} \text{ yr}^{-1}$ obtained for the northwestern Mediterranean characterized by similar dynamical conditions (cf. Levy et al., 1998).

The annual distribution of daily average PP integrated over the euphotic zone (Fig. 14a) suggests that, to a major proportion, the annual production takes place during the spring bloom period with the maximum intensity of $3.5 \text{ g C m}^{-2} \text{ day}^{-1}$. Unfortunately, no data exist to support this value, but there are some field estimates (Fig. 14b) providing water column integrated PP values of $\sim 600 \text{ mg C m}^{-2} \text{ day}^{-1}$ during late February–early March 1995, $\sim 479 \text{ mg C m}^{-2} \text{ day}^{-1}$ during early May 1996 and $\sim 93 \text{ mg C m}^{-2} \text{ day}^{-1}$ during late November 1996. When superimposed on Fig. 13, these values match quite well the model results.

The PP estimates given by Antoine et al. (1995) from their analysis of CZCS data deserve some comments. Although our annual mean PP estimate is very close to theirs, our value is essentially based on

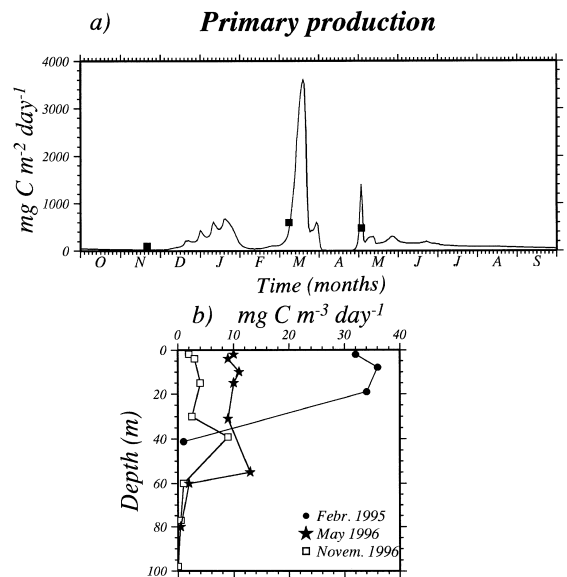


Fig. 14. (a) Simulated and observed annual distributions of the euphotic layer integrated primary production ($\text{mg C m}^{-2} \text{ day}^{-1}$) in the Rhodes gyre, (b) vertical profiles of primary production ($\text{mg C m}^{-3} \text{ day}^{-1}$) measured in the Rhodes gyre at different periods. In (a) the time axis starts at October 1 and ends at September 30.

high PP values of the March bloom. On the contrary, this period is characterized by the lowest PP values ($150 \text{ mg C m}^{-2} \text{ day}^{-1}$) in their analysis and the main contribution comes from the summer period ($350 \text{ mg C m}^{-2} \text{ day}^{-1}$). The low PP estimates from the CZCS data for March is in fact misleading since it is based on averaging of nine images (see Table 2) with extremely low chlorophyll values, as described in the previous section. Their estimate does not even include the contribution of March 15, 1985 data, since they covered the CZCS data set up to 1984.

4. Simulation of Ionian basin ecosystem

4.1. Stratification characteristics

The temperature and salinity distributions for the upper 150 m of the water column of the western

Ionian Sea (Fig. 15a,b) exhibit considerable differences compared to those of the Rhodes basin, especially during the winter season. Contrary to 400 m deep convection in the Rhodes case, the water column deepens at most to 100 m depth as shown by the 15°C isotherm in Fig. 15a and the 37.8 isohaline in Fig. 15b, followed by a sharp salinity gradient at the base of the mixed layer. Because of the presence of the less saline MAW with 37.5 ppt in the near surface levels of the western Ionian Sea, atmospheric cooling can not lead to sufficiently dense water mass formation (over 29 kg/m^3) to break the pycnocline and mix to deeper levels. The mixed layer deepening continues until mid-April, the upper layer water column begins to shallow only after the end of April, as the heating begins to intensify over the region. The period from mid-March to mid-April constitutes a transition period with almost zero net heat flux, as

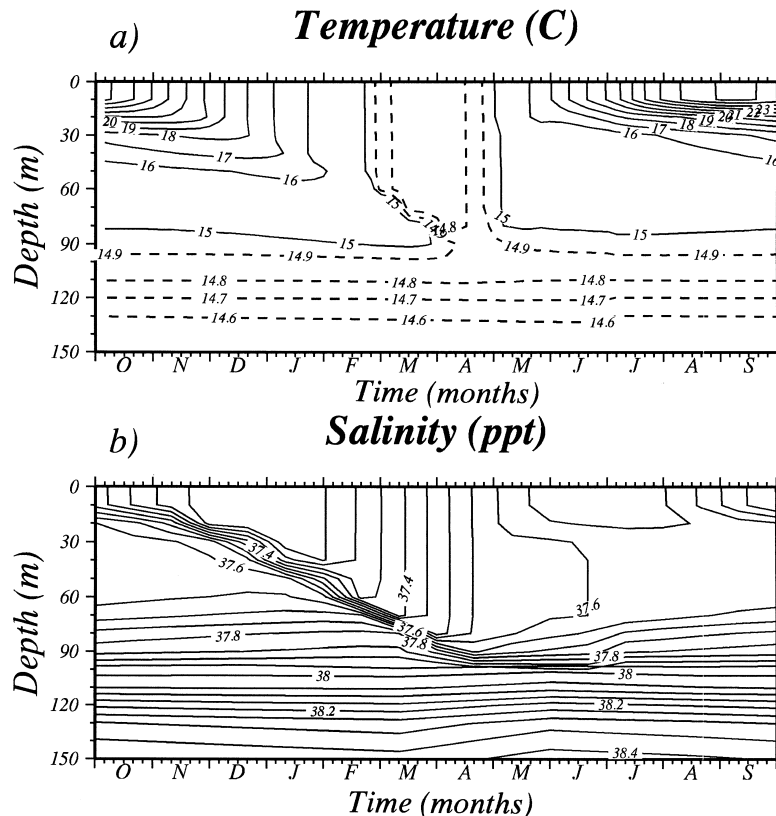


Fig. 15. Simulated annual distributions of (a) temperature and (b) salinity within the upper 150 m depth of the water column in the western Ionian basin. For temperature, contours with continuous lines are at intervals of 1°C , and with broken lines at 0.1°C . For salinity, contours are at intervals of 0.05 ppt. In both plots, the time axis starts at October 1 and ends at September 30.

may be noted by Fig. 2. The water column physical properties reveal two further important differences. The first one is related with the water column stratification below the 100 m depth. The Ionian thermaline structure possesses a strong stratification contrary to the vertically uniform conditions observed in the Rhodes gyre. The second difference is associated with the presence of relatively homogeneous properties from the seasonal thermocline to the 100 m depth in the Ionian gyre whereas the same depth range is characterized by strong stratification in the Rhodes gyre.

The vertical and seasonal variations of the temperature and salinity simulated by the model are supported by observations given by the MODB. Fig. 16 displays the model simulated mixed layer temperature distribution together with the surface temperature data from available observations. The agreement between the model and observations is also quite satisfactory here.

4.2. Biological characteristics

Similar to their physical characteristics, a substantial difference in the water column nitrate distribution of the western Ionian and Rhodes basins is indicated by Fig. 17a. The weak vertical mixing in the winter months implies lack of sufficient nitrate supply from the subsurface levels to support the biological production in the subsequent early spring season. Fig. 17a clearly shows no nitrate accumulation inside the mixed layer during the winter. Whatever nitrate is entrained into the mixed layer from the subsurface levels is consumed immediately in the

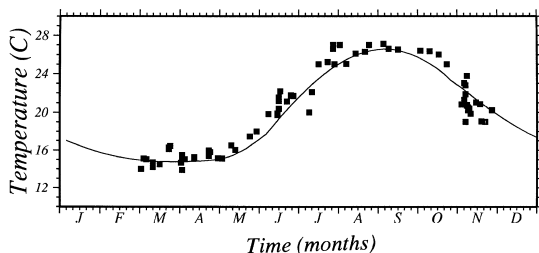


Fig. 16. Simulated annual mixed layer temperature distribution (continuous line) and the observed sea surface temperatures (solid squares) taken from Mediterranean Oceanographic Data Base system for the western Ionian basin.

phytoplankton production process. This is initiated during mid-January and gradually increased to its peak at the end of February (Fig. 17b). The phytoplankton biomass can attain in this period only 0.25 mmol N/m^3 which is an order of magnitude lower than the typical spring bloom values of the Rhodes simulation. The decline of the phytoplankton bloom occurs during March. April is the period of intense nitrogen cycling followed by regenerated production during early May and its continuation at the subsurface levels below the thermocline in June with the maximum biomass of 0.16 mmol N/m^3 . The subsurface production can be traced in the nitrate field by the slight increase of isolines during early summer period (Fig. 17a). The annual distribution of zooplankton stock (Fig. 17c) shows a maximum biomass value of about 0.15 mmol N/m^3 . This is again one order of magnitude smaller than the values obtained in the Rhodes simulations.

The way in which the intensity of vertical mixing controls timing of the early spring phytoplankton bloom was described earlier in Oguz et al. (1996) in the context of the Black Sea plankton production model. It was shown that even though the light and nutrient conditions may be favorable for initiation of the bloom in winter, it can be delayed depending on the intensity of the vertical mixing. In the absence of any zooplankton grazing pressure and other losses due to phytoplankton mortality and excretion during winter, the vertical mixing is the only sink term which can balance the production. The initiation of phytoplankton bloom therefore depends on the relative intensities of these two processes during winter–early-spring period. The biological production will be initiated whenever the vertical mixing weakens and its magnitude is exceeded by that of the production term. In our simulations, the Rhodes case is a good example for the delay of the bloom until the intense mixing weakens during the winter. The other region having similar features is the northwestern Mediterranean deep-water formation area where prevention of the bloom by strong vertical mixing was referred to as ‘‘deep mixing limitation of the bloom’’ (Levy et al., 1998). The Ionian case, on the contrary, favors biological conditions weakly controlled by the vertical mixing. Thus, the bloom begins earlier in winter and intensifies gradually until the net limitation factor $\Phi(I, N, A)$ given by Eq. (8)

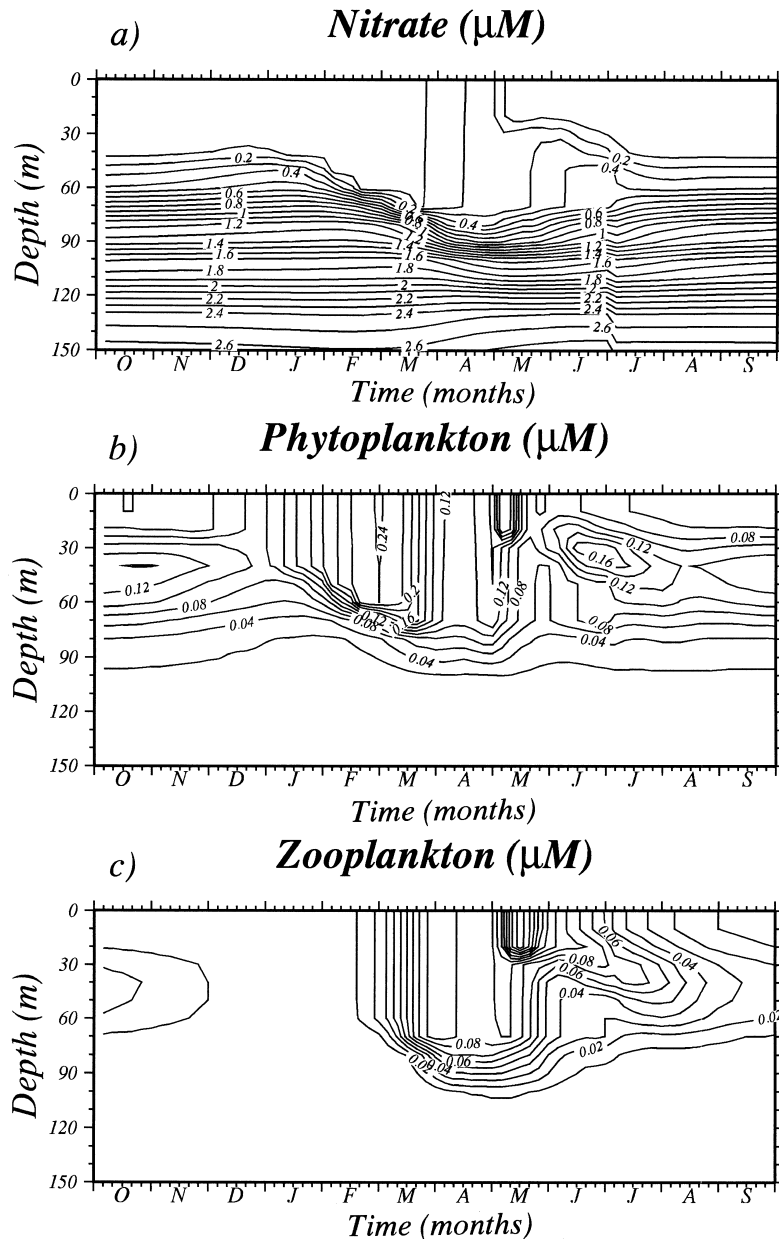


Fig. 17. Simulated annual distributions of (a) nitrate, (b) phytoplankton and (c) zooplankton for the western Ionian basin within the upper 150 m depth of the water column. Units are in mmol N m^{-3} . For nitrate, the contours are at intervals of $0.1 \text{ mmol N m}^{-3}$, for phytoplankton at $0.02 \text{ mmol N m}^{-3}$ and for zooplankton at $0.01 \text{ mmol N m}^{-3}$. In all plots, the time axis starts at October 1 and ends at September 30.

attains its maximum value. The monthly mean CZCS chlorophyll data (Fig. 18), given as the average of pixels inside our analysis area, seem to support such

an extended period of increased phytoplankton activity. The magnitude of CZCS chlorophyll values also compare well with the surface phytoplankton biomass

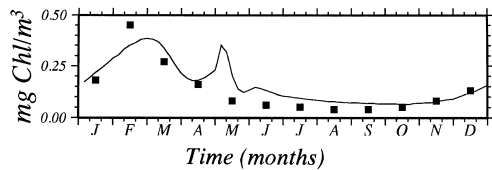


Fig. 18. Simulated annual surface chlorophyll *a* (in mg Chl/m³) distribution for the western Ionian sea (continuous line) and the CZCS-derived surface chlorophyll *a* concentrations averaged from the pixels located in the shaded region shown in Fig. 1a.

values in Fig. 17b by using a conversion factor of 1 mmol nitrogen being equivalent to 1.2 mg Chl as before.

The annual budget and intercompartmental transfer rates for the Ionian simulation is also shown in Fig. 13 by the numbers in parentheses. The budget indicates that only 4.1 g C m⁻² yr⁻¹ nitrate enters the euphotic zone from the deeper layers. The contribution of recycled nitrogen from detrital breakdown and plankton excretion are 3.9 and 2.0 g C m⁻² yr⁻¹, respectively, which all together sum up to a total PP rate of 10.1 g C m⁻² yr⁻¹. This is an extremely low value, but is considered to be typical for oligotrophic sites of the Eastern Mediterranean. Applying the model of CCM (1998) to the same region for the interpretation and analysis of the hydrographic and nutrient data collected during October 1991 and April 1992 surveys, Civitarese et al. (1996) obtained a mean PP value of 11.5 g C m⁻² yr⁻¹, which is very close to our result.

5. Summary and discussion

The biological productivity of the eastern Mediterranean is studied by concentrating on two particular regions with contrasting physical characteristics. One of them is the Rhodes cyclonic gyre of the Northern Levantine Sea known to be a major, persistent sub-basin scale feature of the Eastern Mediterranean between the Rhodes and Cyprus islands. The other is the anticyclonic gyre of the western Ionian Sea extending meridionally to the east of the Sicily Straits. Simulations are carried out using a one-dimensional vertically resolved physical–biological model. It couples the upper ocean physical model with the ecosystem dynamics of the

biological model through the specification of vertical eddy diffusivity using the Mellor–Yamada level 2.5 turbulence parameterization. The biological model includes aggregated compartments of phytoplankton, zooplankton and detritus, as well as ammonium and nitrate. The use of nitrate as a limiting nutrient alone might be questionable in the Eastern Mediterranean, as the recent data tend to support phosphate limitation within the euphotic zone (~100 m) of the Rhodes gyre region (Zohary and Robarts, 1998). Our model results therefore tend to overestimate the primary production and phytoplankton biomass to some extent. The role of phosphate as an additional nutrient which limits biological production in the model is presently under investigation.

The Rhodes basin reveals a well-pronounced cyclonic circulation providing strong exchange between the surface and intermediate-deep waters through upwelling and intense vertical convective overturning processes. Therefore, the water column below the seasonal thermocline is typically characterized by relatively cold, saline and dense waters. On the contrary, the western anticyclonic Ionian gyre possesses very limited surface-intermediate water interactions because of the presence of less saline Modified Atlantic Waters (MAW) within the upper 100 m layer. The strong stratification introduced by the presence of MAW and LIW underneath prevents deep penetration of the vertical convection and, subsequently, the nutrient supply from deeper levels. Because of these two contrasting dynamical regimes, the two basins reveal quite different vertical nutrient structures. The upper levels of the Rhodes gyre are always rich in nitrate. On the contrary, the nitrate concentrations between the 100 and 300 m depths in the western Ionian anticyclone are only half of those of the Rhodes gyre. In our simulations, these prevailing physical conditions are shown to lead to high biological production in the Rhodes area. The annual primary production is estimated as 97.4 g C m⁻² yr⁻¹. This value is comparable with those of the Aegean, Adriatic and northwestern Mediterranean basins (Antoine et al., 1995). The corresponding value obtained by the analysis of the CZCS data by Antoine et al. (1995) is 87.6 g C m⁻² yr⁻¹. Although these two numbers are consistent with each other, our model tends to underestimate the summer PP whereas their value does not incorporate the

contribution of early winter and early spring blooms. The simulations also demonstrate how the physical conditions in the western Ionian basin limit the biological production. The primary production in the western Ionian Sea amounts only to 10% of the Rhodes' case. Therefore, these two basins represent biologically two end members of the Eastern Mediterranean. The annual production cycle also differs slightly in these two basins. The Rhodes gyre possesses a "classical" production cycle consisting of a strong early spring bloom, a weaker late autumn–early winter bloom and subsurface production during summer. In the western Ionian basin, the two blooms are merged with each other to form a long lasting, gradually evolving winter bloom starting from the beginning of January to the end of March. The early spring bloom of the Rhodes gyre, on the other hand, has a shorter lifetime, grows and decays exponentially.

Our annual primary production estimates for both the Rhodes and western Ionian basins may be modified by several processes not included within the one-dimensional approach. In the Rhodes case, the upward advective flux of nitrate associated with the permanent cyclonic circulation system is expected to promote stronger summer production below the seasonal thermocline. The atmospheric input and nitrogen fixation might be responsible for triggering biological activity by enhancing nitrogen concentration inside the mixed layer. The lateral advection of flow through eddy fluxes might provide additional nitrate supply which enhance the primary production. Moreover, representation of phytoplankton and zooplankton by single aggregated compartments introduces strong limitation on the phytoplankton–zooplankton interactions during the year. On the other hand, introducing size-fractionation for these groups enhances the subsurface production during the summer and autumn seasons as we experienced in our Black Sea biological modeling studies (Oguz et al., 1998, 1999). This is, however, not yet feasible for the Mediterranean Sea because of the lack of sufficient data to represent the details of complicated trophic interactions.

Comparison of the model simulations with the available observations is fairly satisfactory, although the observations can only provide support for the main features of the Rhodes and western Ionian

ecosystems. In this respect, this study clearly demonstrates the extreme importance and necessity of carrying out systematic intensive and extensive biogeochemical observational studies within the framework of international, multi-institutional research efforts. Furthermore, ability of the one-dimensional model in simulating essential features of two very distinct ecosystems using a common set of parameters encourages its three-dimensional implementation for the entire eastern Mediterranean.

Acknowledgements

E. Napolitano gratefully acknowledges the support provided by the Universita' di Messina and Istituto Universitario Navale Environmental Marine Sciences Joint PhD Program as a visiting fellow at MIT. P. Malanotte-Rizzoli and T. Oguz acknowledge the NSF support OCE-9633145. The authors thank the reviewers whose comments led to considerable improvement in the manuscript.

References

- Andersen, V., Nival, P., 1988. Modele d'ecosysteme pelagique des eaux cotieres de la Mer Ligure. *Oceanol. Acta* 9, 211–217, Pelagic Mediterranean Oceanography.
- Antoine, D., Morel, A., Andre, J.-M., 1995. Algal pigment distribution and primary production in the eastern Mediterranean as derived from coastal zone color scanner observations. *J. Geophys. Res.* 100, 16193–16209.
- Bergamasco, A., Oguz, T., Malanotte-Rizzoli, P., 1999. Modeling dense water mass formation and winter circulation in the northern and central Adriatic Sea. *J. Mar. Syst.* 20, 279–300.
- Berland, R.B., Benzhitski, A.G., Burlakova, Z.P., Georgieva, L.V., Izmetieva, M.A., Kholodov, V.I., Maestrini, S.Y., 1998. Hydrological structure and particulate matter distribution in Mediterranean seawater during summer. *Oceanol. Acta* 9, 163–177, Pelagic Mediterranean Oceanography.
- Brasseur, P., Beckers, J.M., Brankart, J.M., Schoenauen, R., 1996. Seasonal temperature and salinity fields in the Mediterranean Sea: climatological analyses of a historical data set. *Deep-Sea Res.*, Part I 43, 159–192.
- Civitarese, G., Crise, A., Crispi, G., Mosetti, R., 1996. Circulation effects on nitrogen dynamics in the Ionian Sea. *Oceanol. Acta* 19, 609–622.
- Crise, A., Crispi, G., Mauri, E., 1998. A seasonal three-dimensional study of the nitrogen cycle in the Mediterranean Sea: Part I. Model implementation and numerical results. *J. Mar. Syst.* 18, 287–312.

- Crispi, G., Crise, A., Mauri, E., 1999. A seasonal three-dimensional study of the nitrogen cycle in the Mediterranean Sea. *J. Mar. Syst.* 20, 357–379.
- Doney, S.C., Glover, D.M., Najjar, R.G., 1996. A new coupled one-dimensional biological–physical model for the upper ocean: applications to the JGOFS Bermuda Time Series Study (BATS) site. *Deep-Sea Res.* 43, 591–624.
- Ediger, D., 1995. Interrelationships among primary production, chlorophyll and environmental conditions in the northern Levantine basin. PhD thesis, Middle East Technical University, Institute of Marine Sciences, Erdemli, Icel, Turkey, 187 pp.
- Ediger, D., Tugrul, S., Polat, C.S., Yilmaz, A., Salihoglu, I., 1999. Abundance and elemental composition of particulate matter in the upper layer of the northeastern Mediterranean. In: Malanotte-Rizzoli, P., Eremeev, V.N. (Eds.), *The Eastern Mediterranean as a Laboratory Basin for the Assessment of Contrasting Ecosystems*. Kluwer Academic Publishers, pp. 241–266.
- Ediger, D., Yilmaz, A., 1996. Characteristics of deep chlorophyll maximum in the northeastern Mediterranean with respect to environmental conditions. *J. Mar. Syst.* 9, 291–303.
- Fasham, M.J.R., Ducklow, H.W., Mckelvie, S.M., 1990. A nitrogen-based model of plankton dynamics in the oceanic mixed layer. *J. Mar. Res.* 48, 591–639.
- Jassby, A.D., Platt, T., 1976. Mathematical formulation of the relationship between photosynthesis and light for phytoplankton. *Limnol. Oceanogr.* 21, 540–547.
- Kuhn, W., Radach, G., 1997. A one-dimensional physical–biological model study of the pelagic nitrogen cycling during the spring bloom in the northern North Sea (FLEX'76). *J. Mar. Res.* 55, 687–734.
- Lascaratos, A., Nittis, K., 1998. A high-resolution three-dimensional numerical study of intermediate water formation in the Levantine Sea. *J. Geophys. Res.* 103, 18497–18511.
- Levy, M., Memery, L., Andre, J.-M., 1998. Simulation of primary production and export fluxes in the northwestern Mediterranean Sea. *J. Mar. Res.* 56, 197–238.
- Malanotte-Rizzoli, P., Manca, B., Ribera, M., Theocharis, A., Bergamasco, A., Bregant, D., Budillon, G., Civitarese, G., Georgopoulos, D., Michelato, A., Sansone, E., Scarazzato, P., Souvermezoglou, E., 1997. A synthesis of the Ionian Sea hydrography, circulation and water mass pathways during POEM-Phase I. *Prog. Oceanogr.* 39, 153–204.
- May, P.W., 1982. Climatological heat flux estimates of the Mediterranean Sea: Part I. Winds and wind stresses. Report 54, NORDA, NSTL Station, 7539529, 56 pp.
- McClain, C.R., Arrigo, K., Tai, K.-S., Turk, D., 1996. Observations and simulations of physical and biological processes at ocean weather station P, 1951–1980. *J. Geophys. Res.* 101, 3697–3713.
- McGullicuddy, D.J., Mccarthy, J.J., Robinson, A.R., 1995. Coupled physical and biological modeling of the spring bloom in the North Atlantic: I. Model formulation and one-dimensional bloom processes. *Deep-Sea Res., Part I* 42, 1313–1357.
- Mellor, G.L., 1990. User's Guide for a Three-Dimensional, Primitive Equation Numerical Ocean Model. *Prog. in Atmos. Ocean Sci.*, Princeton Univ., Princeton, NJ, 35 pp.
- Oguz, T., Ducklow, H.W., Malanotte-Rizzoli, P., Murray, J.W., 1998. Simulations of the Black Sea pelagic ecosystem by one-dimensional vertically resolved physical–biochemical models. *Fish. Oceanogr.* 7, 300–304.
- Oguz, T., Ducklow, H.W., Malanotte-Rizzoli, P., Murray, J.W., Vedernikov, V.I., Unluata, U., 1999. A physical–biochemical model of plankton productivity and nitrogen cycling in the Black Sea. *Deep-Sea Res., Part I* 46, 597–637.
- Oguz, T., Ducklow, H.W., Malanotte-Rizzoli, P., Tugrul, S., Nezlin, N., Unluata, U., 1996. Simulation of annual plankton productivity cycle in the Black Sea by a one-dimensional physical–biological model. *J. Geophys. Res.* 101, 16585–16599.
- Ozsoy, E., Hect, A., Unluata, U., Brenner, S., Oguz, T., Bishop, J., Latif, M.A., Rosentraub, Z., 1991. A review of the Levantine Basin circulation and its variability during 1985–1988. *Dyn. Atmos. Oceans* 15, 421–456.
- Ozsoy, E., Hect, A., Unluata, U., Brenner, S., Sur, H.I., Bishop, J., Oguz, T., Rosentraub, Z., Latif, M.A., 1993. A synthesis of the Levantine Basin circulation and hydrography. *Deep-Sea Res.* 40, 1075–1119.
- Rabitti, S., Bianchi, F., Boldrin, A., Daros, L., Socal, G., Totti, C., 1994. Particulate matter and phytoplankton in the Ionian Sea. *Oceanol. Acta* 17, 297–307.
- Robinson, A.R., McGillicuddy, D.J., Calman, J., Ducklow, H.W., Fasham, M.J.R., Hoge, F.E., Leslie, W.G., Mccarthy, J.J., Podewski, S., Porter, D.L., Saure, G., Yoder, Y.A., 1993. Mesoscale and upper ocean variabilities during the 1989 JGOFS bloom study. *Deep-Sea Res., Part II* 40, 9–35.
- Salihoglu, I., Saydam, C., Basturk, O., Yilmaz, K., Gocmen, D., Hatipoglu, E., Yilmaz, A., 1990. Transport and distribution of nutrients and chlorophyll *a* by mesoscale eddies in the northeastern Mediterranean. *Mar. Chem.* 29, 375–390.
- Souvermezoglou, K., Hatzigeorgiou, E., Pampidis, I., Siapsali, K., 1992. Distribution and seasonal variability of nutrients and dissolved oxygen in the northeastern Ionian Sea. *Oceanol. Acta* 15, 585–594.
- Sur, H.I., Ozsoy, E., Unluata, U., 1993. Simultaneous deep and intermediate depth convection in the Northern Levantine Sea, winter 1992. *Oceanol. Acta* 16, 33–433.
- Yilmaz, A., Ediger, D., Basturk, O., Tugrul, S., 1994. Phytoplankton fluorescence and deep chlorophyll maxima in the northeastern Mediterranean. *Oceanol. Acta* 17, 69–77.
- Yilmaz, A., Tugrul, S., 1999. The effect of cold- and warm-core eddies on the distribution and stoichiometry of dissolved nutrients in the northeastern Mediterranean. *J. Mar. Syst.* 16, 253–268.
- Zohary, T., Robarts, R.D., 1998. Experimental study of microbial P limitation in the eastern Mediterranean. *Limnol. Oceanogr.* 43, 387–395.